Supporting Information

Iron-cobalt nanoparticles dispersed in indium-based MIL-68-derived carbon nanosticks for water oxidation

Haoran Wang, Nan Li, Yuting Fu, Junliang Chen, Jie Liu, Yuandong Yang, Shaojie Xu and Jinjie Qian*

Key Laboratory of Carbon Materials of Zhejiang Province, College of Chemistry and Materials Engineering, Wenzhou University, Wenzhou, Zhejiang, 325000, P. R. China

657000, PR China

*Corresponding Author.

E-mail address: jinjieqian@wzu.edu.cn

1. Experimental

1.1 Reagents and Materials.

All chemicals and solvents are used as purchased in this work without further purification: Terephthalic acid (H_2BDC, 97%), cobalt nitrate ($Co(NO_3)_2 \cdot 6H_2O$, AR, 99%, Aladdin), ferric nitrate ($Fe(NO_3)_3 \cdot 6H_2O$, AR, 99%, Aladdin), indium nitrate ($In(NO_3)_2 \cdot 6H_2O$, AR, 99%, Aladdin), deionized water (DI H_2O, 18 MΩ), N,N'-dimethyformamide (DMF, ≥99.8%, Aladdin), ethanol (EtOH, >99%, GC, Aladdin) and Nafion (5 wt%, DuPont).

1.2 Synthesis of MIL-68

After 30 minutes of ultrasonic treatment, the $In(NO_3)_3 \bullet 6H_2O$ (250 mg) and H_2BDC (125 mg) are completely dissolved in solution of DMF (6.5 mL). Then, the homogeneous solution is transferred to a 25 mL glass bottle and placed in the oven at 85 ^oC for 6 hours. The obtained crystals are soaked in EtOH for 24 hours to replace the guest molecules and washed three times with EtOH to obtain the pure **MIL-68**.

1.3 Synthesis of MIL-68-FeCo/MIL-68-Fe/MIL-68-Co

$Co(NO_3)_2 \cdot 6H_2O$ (72 mg)+$Fe(NO_3)_3 \cdot 6H_2O$ (28 mg) and **MIL-68** (30 mg) are mixed with DMF (3 mL) and H_2O (3 mL) in a pressure-resistant pipe, then heated at 120 °C for 6.5 hours. After cooling to room temperature, the product is collected by centrifugation at 10000 rpm, then washed three times with ethanol and finally vacuum-dried at 85 °C overnight.

The synthesis scheme for **MIL-68-Co** and **MIL-68-Fe** follows the same steps as the scheme outlined for **MIL-68-FeCo**, with the addition of $Co(NO_3)_2 \cdot 6H_2O$ (100 mg) and $Fe(NO_3)_3 \cdot 6H_2O$ (28 mg), respectively.

1.4 Synthesis of MIL-68-C/MIL-68-Fe-C/MIL-68-Co-C/MIL-68-FeCo-C

The as-obtained **MIL-68/MIL-68-Fe/MIL-68-Co/MIL-68-FeCo** is transferred into a chemical vapour deposition (CVD) tube furnace and carbonized at 850 ^{o}C for 2 hours under the Ar atmosphere (the heating rate of 10 ^{o}C min^{-1}). The resultant samples are denoted as **MIL-68-C/MIL-68-Fe-C/MIL-68-Co-C/MIL-68-FeCo-C**.

2 Apparatus and Physical Measurement.

2.1 General Instruments.

Scanning electron microscopy (SEM) data are obtained within a JSM-6700F field emission scanning electron microscope at 10 kV. High-resolution transmission electron microscope (HR-TEM) and energy dispersive spectroscopy (EDS) are collected on a JEOL JEM2100F microscope at a high voltage of 200 kV. N_2 sorption is performed in the Accelerated Surface Area and Porosimetry System 2020 (ASAP 2020) at 77 K. The powder X-ray diffraction patterns (PXRD) are acquired with a Bruker D8 Advance using Cu Kα radiation (0.154 nm). Raman spectra are obtained in Renishaw instrument (in Via-Reflex) with the 532 nm wavelength. X-ray photo electron spectroscopy (XPS) characterizations are carried out on a high resolution electron energy analyzer (Gamma data-Scienta SES 2002) using monochromatic Al Kα X-rays.

2.2 Electrochemical Characterizations.

All electrochemical data are collected by using a CHI760E and/or Autolab electrochemical workstation. The OER measurements are tested in 1.0 M KOH solution by utilizing a typical three-electrode system, the GCE (glass carbon electron) with catalyst ink, a platinum net, and a Hg/HgO electrode as the working, counter, and reference electrodes, respectively. Meanwhile, we chose Hg/HgO as the reference electrode to guarantee accuracy and repeatability in the alkaline medium. All

electrochemical tests in our work are performed without iR corrected. We dispersed 5 mg of target powder with 50 μL of Nafion (5%), 150 μL DI H_2O and 300 μL of ethanol, followed by the ultrasonic treatment for 2 h, and then a 6 μL catalyst ink is dropped on the surface of a GCE electrode and allowed to dry under ambient conditions for 2-3 h. On the contrary, the cyclic voltammogram (CV) is conducted at a scan rate of 10/50 mV s^{-1}; meanwhile, the linear sweep voltammetry (LSV) is recorded at a scan rate of 5 mV s^{-1}, and the electrochemical impedance spectroscopy (EIS) measurements are tested at the frequencies ranging from 10^5 to 10^{-1} Hz, with 1.075 V (*vs.* RHE). The electrochemical double layer capacitance (C_{dl}) curves of different samples are measured by using CVs in a non-Faradaic region (0.95-1.04 V vs RHE) at different scan rates of 20, 40, 60, 80, 100 and 120 mV s^{-1}. Electrocatalytic stability is tested using the Amperometric i-t curve test at a consistent potential of 1.55 V (vs. RHE) for 20 h. All potentials of electrochemical measurement are transferred to the reversible hydrogen electrode (RHE) scale by the following equation: $E_{RHE}=E_{Hg/HgO}+(0.059*pH)+0.197$, The overpotential (η) is calculated as follows: η=E(V vs. RHE)-1.23, according to O_2/H_2O equilibrium (1.23 V vs. RHE). The Tafel slope is transferred according to Tafel equation as follows: $\eta=b\cdot\log(j/j_0)$.

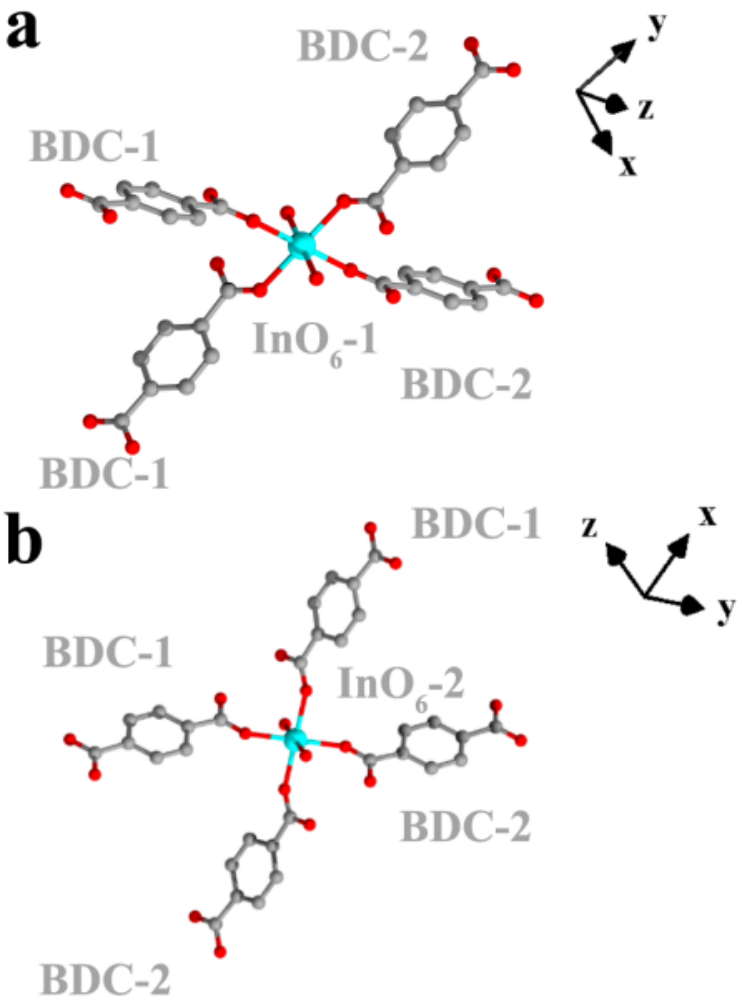

Figure S1. Coordination environments of two types of secondary building units of a) InO_6-1; b) InO_6-2 in the In-based MIL-68.

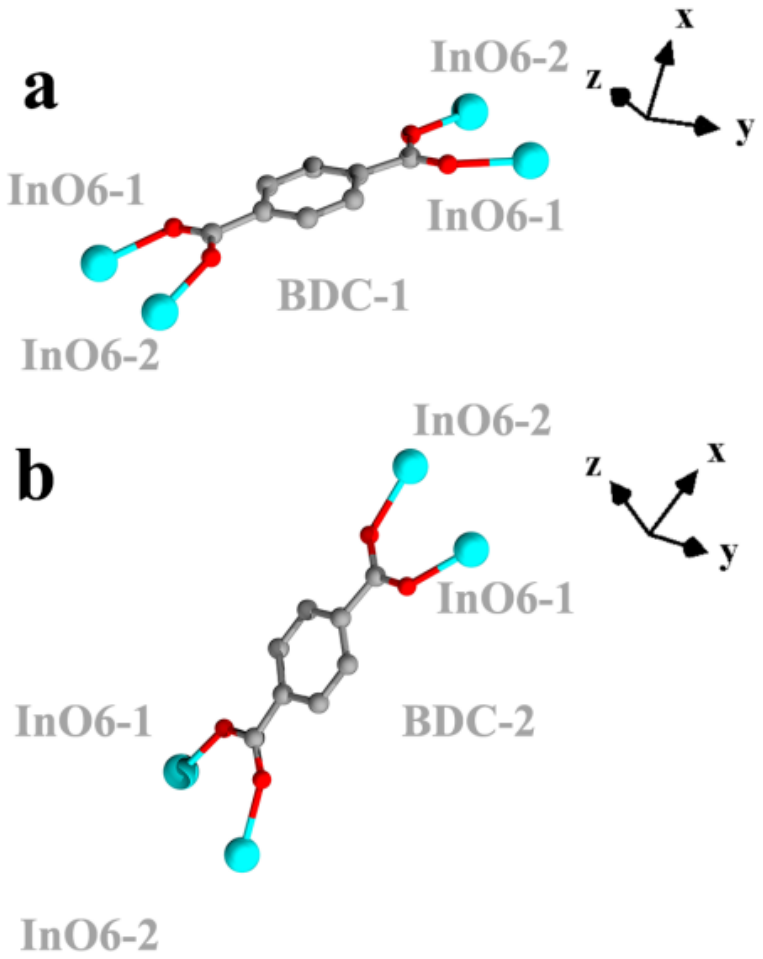

Figure S2. Coordination environments of two types of deprotonated BDC^{2-} ligands of a) BDC-1; b) BDC-2 in the In-based MIL-68.

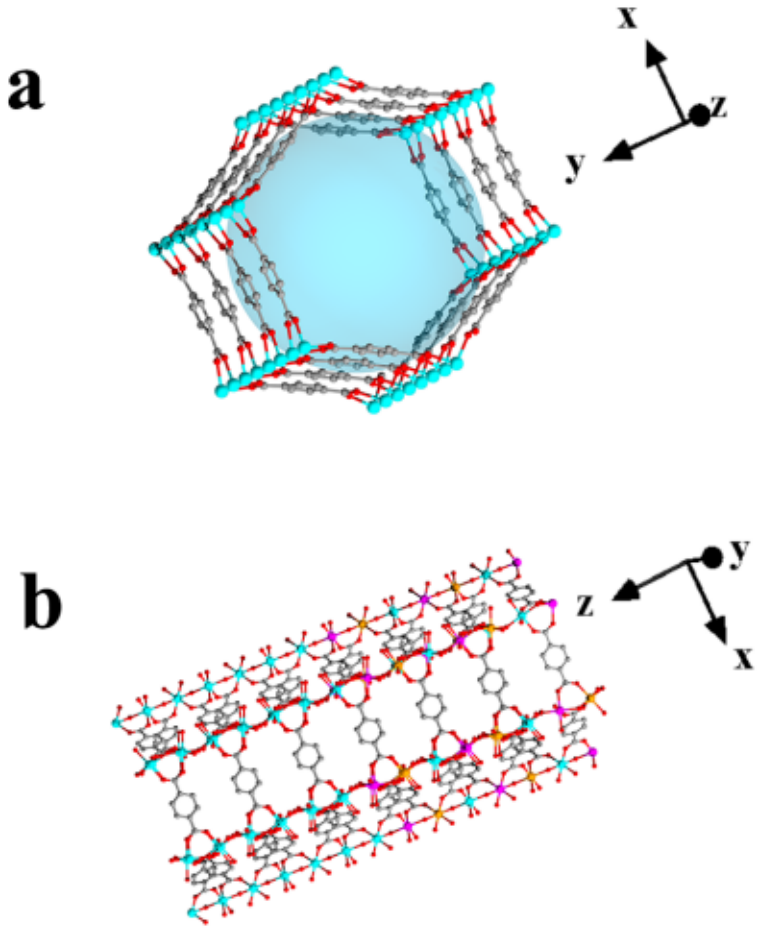

Figure S3. The side views of a) undoped MIL-68 and b) FeCo-doped MIL-68.

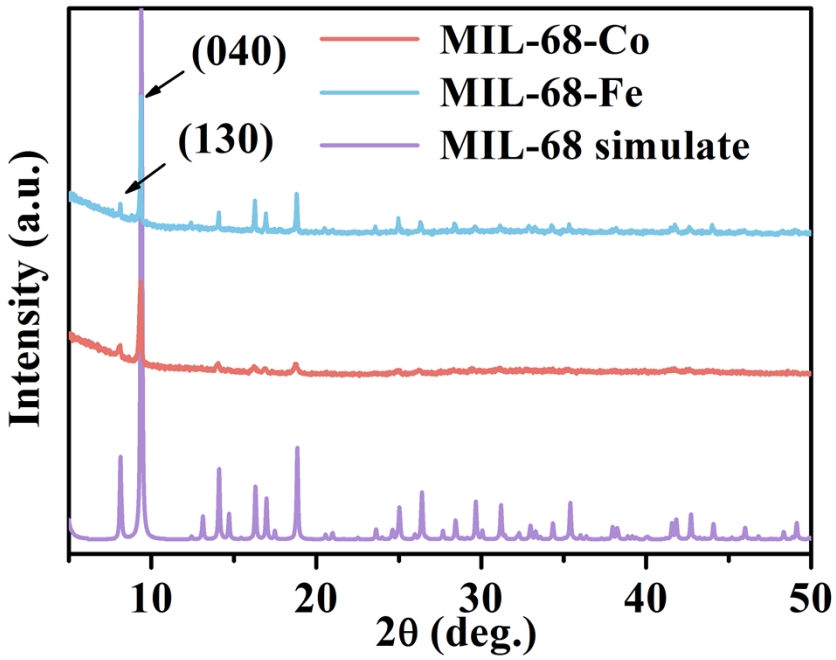

Figure S4. The PXRD patterns of MIL-68-Co and MIL-68-Fe.

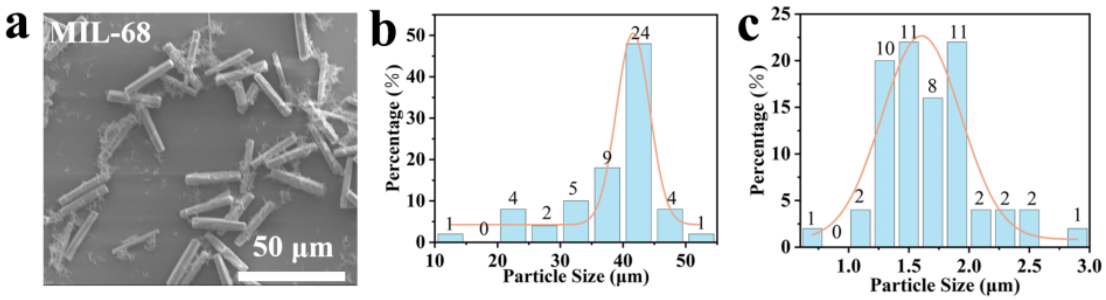

Figure S5. a) The SEM image of MIL-68; b-c) Particle size distribution of MIL-68.

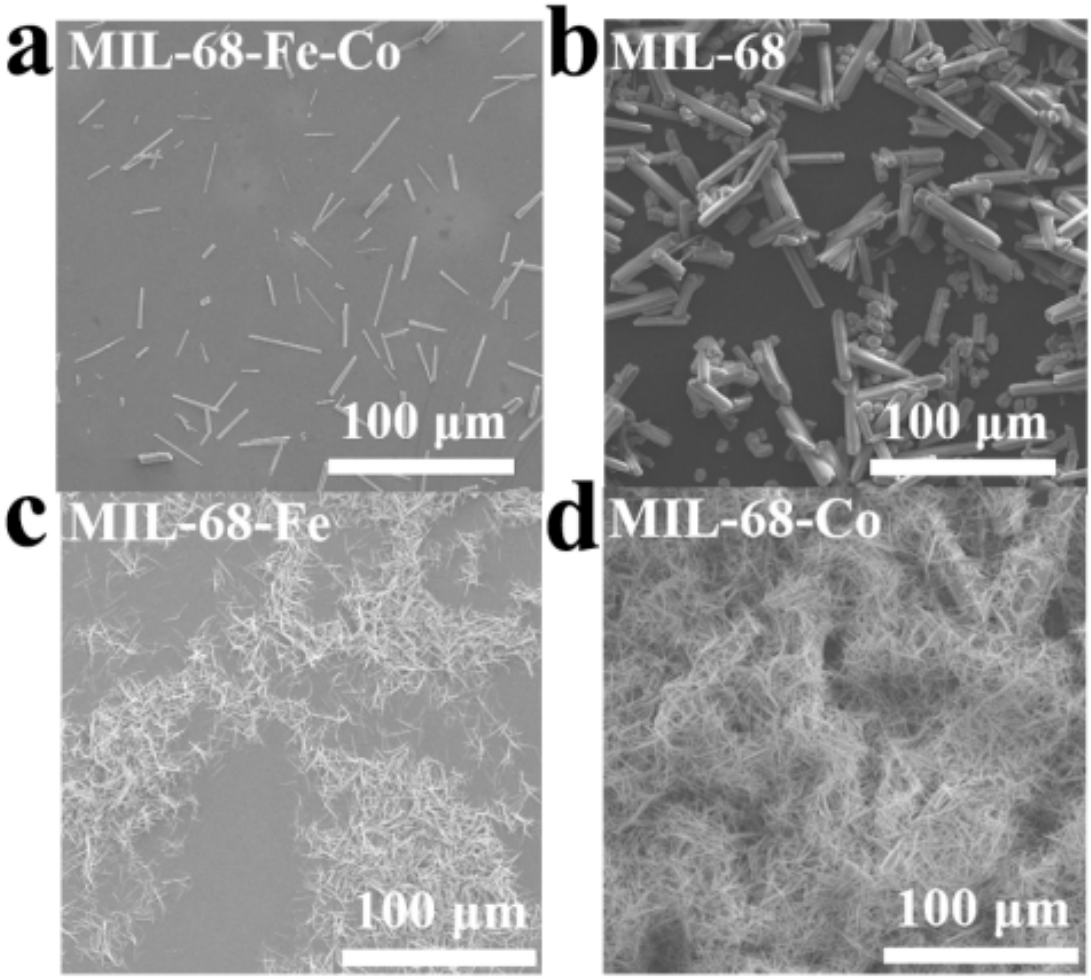

Figure S6. The SEM images of a) MIL-68-FeCo; b) MIL-68; c) MIL-68-Fe and d) MIL-68-Co.

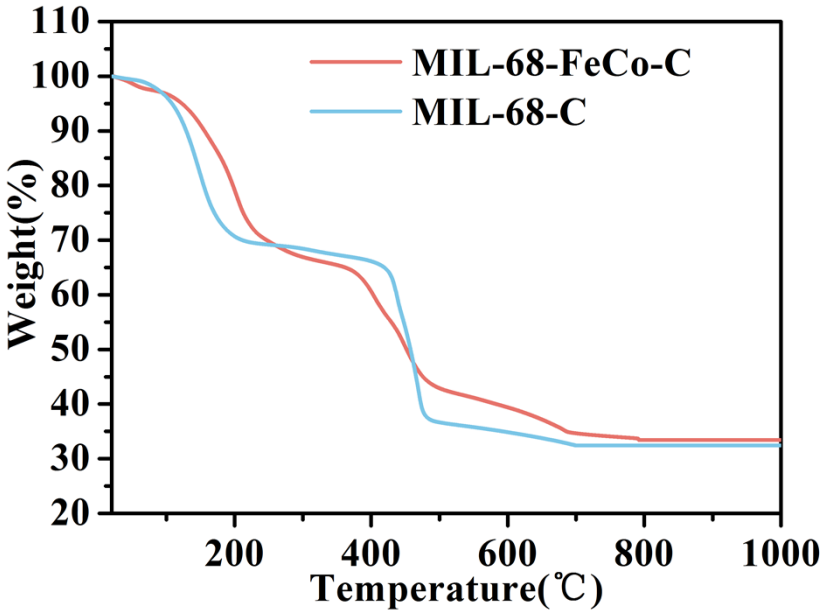

Figure S7. The TGA curves of MIL-68-FeCo-C and MIL-68-C.

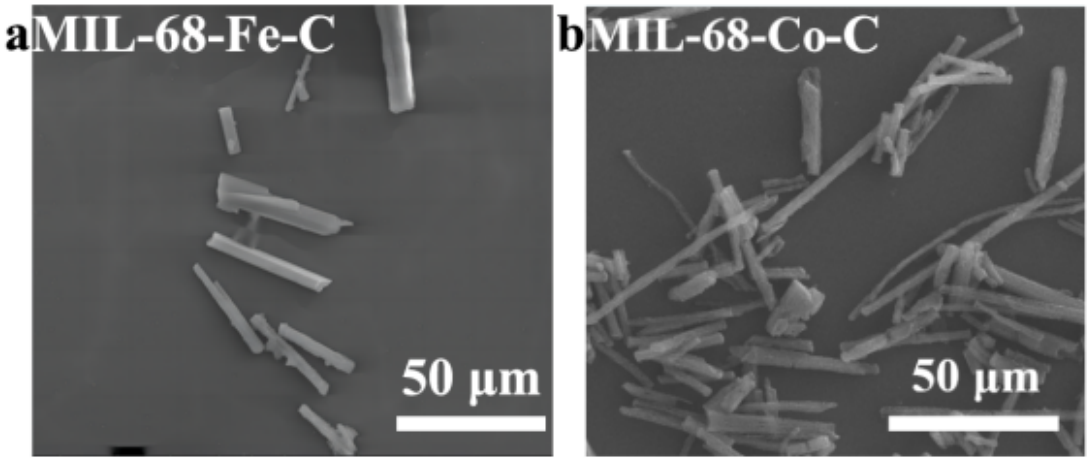

Figure S8. The SEM images of a) MIL-68-Fe-C; b) MIL-68-Co-C.

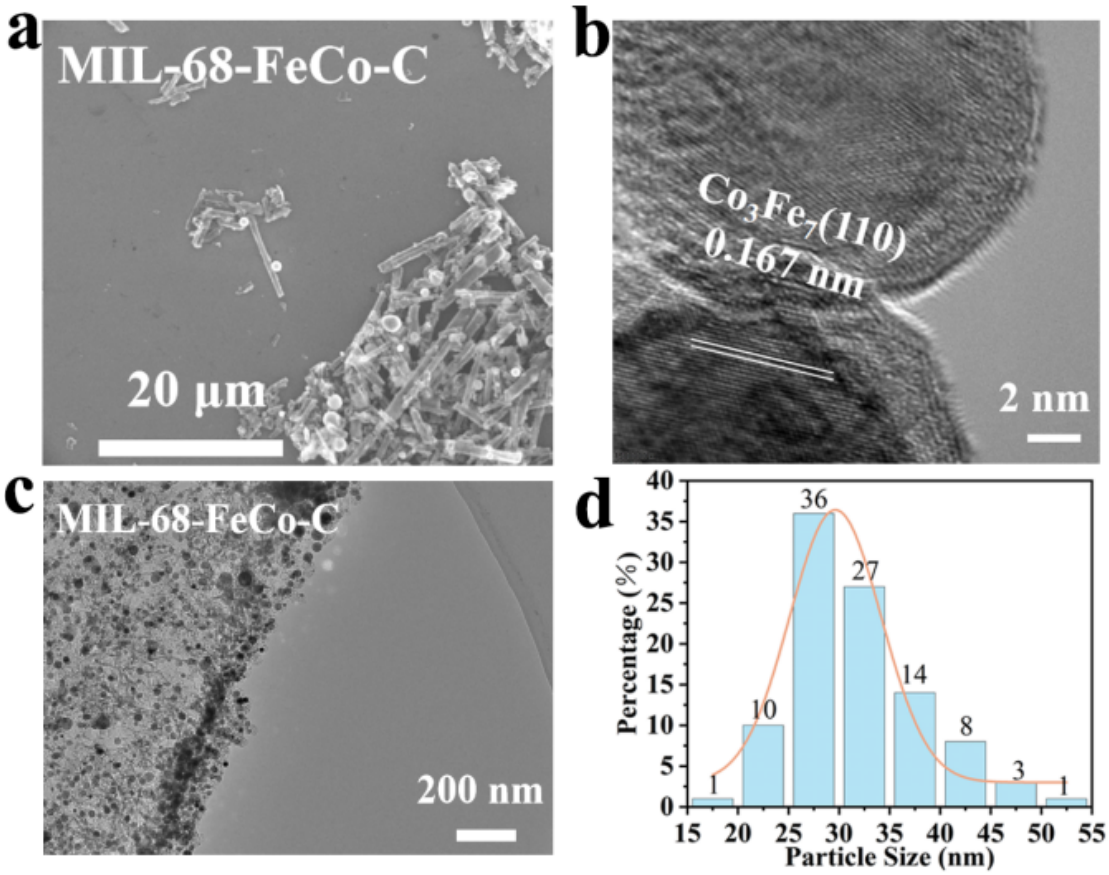

Figure S9. The SEM images of a) MIL-68-FeCo-C; b-c) TEM image of MIL-68-FeCo-C; d) Particle size distribution of FeCo alloy nanoparticles in MIL-68-FeCo-C.

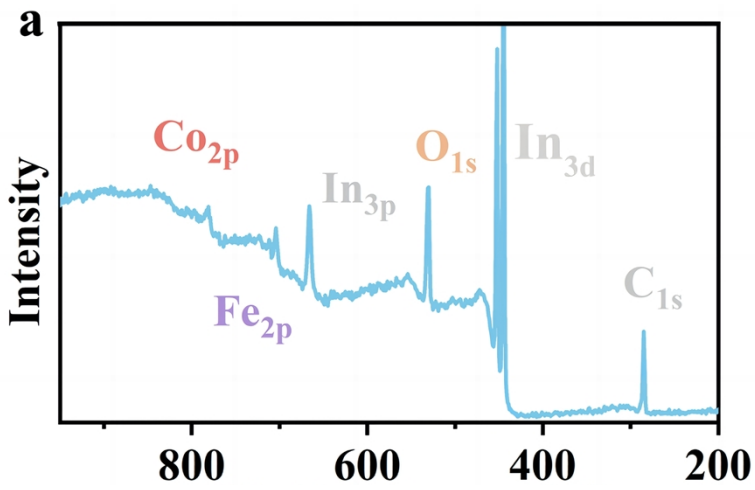

Figure S10. The full survey XPS spectrum of MIL-68-C-FeCo-C.

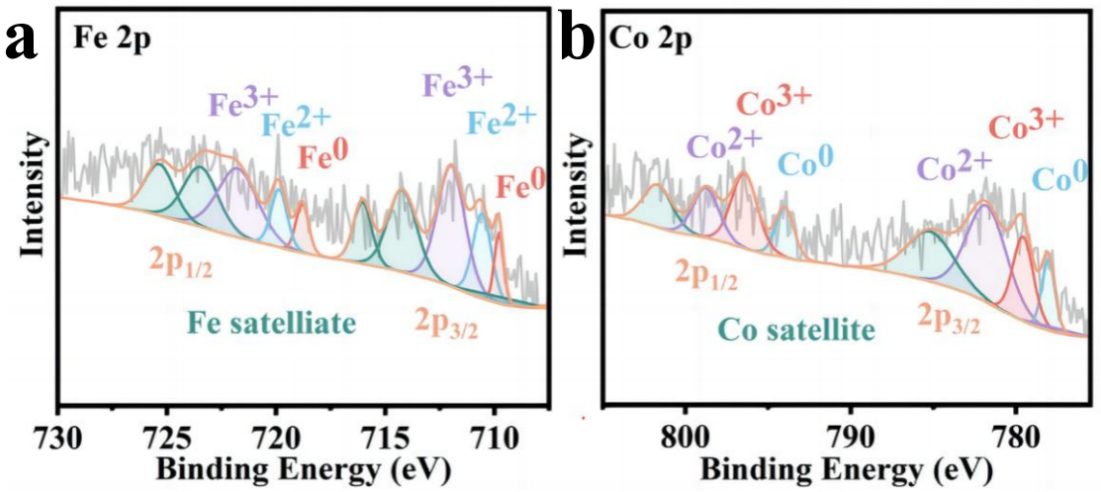

Figure S11. The high-resolution XPS spectra of (a) Fe 2p and (b) Co 2p for MIL-68-C-FeCo-C.

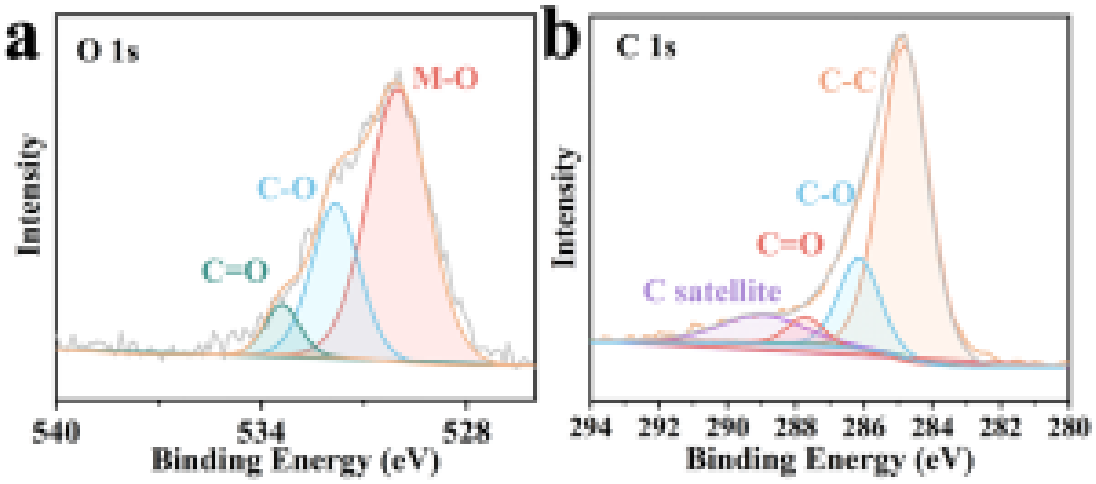

Figure S12. The high-resolution XPS spectra of (a) O 1s and (b) C 1s for MIL-68-C-FeCo-C.

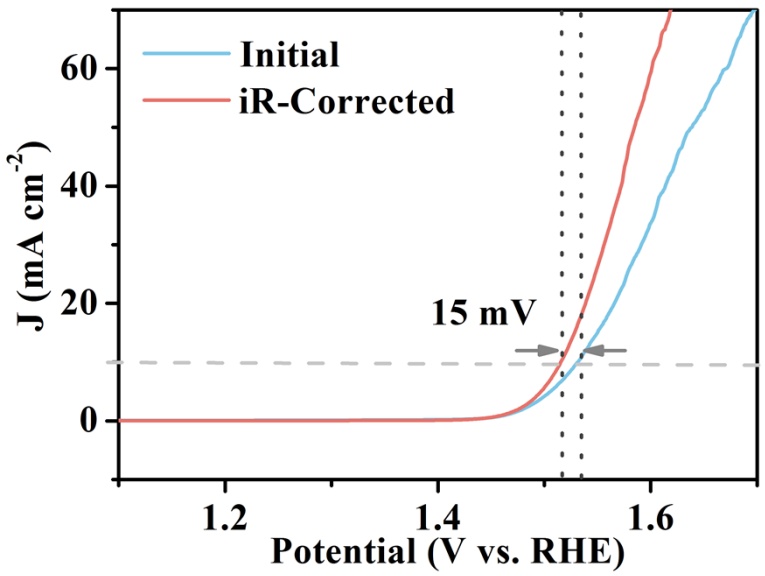

Figure S13. The LSV curves before and after iR-Corrected**.**

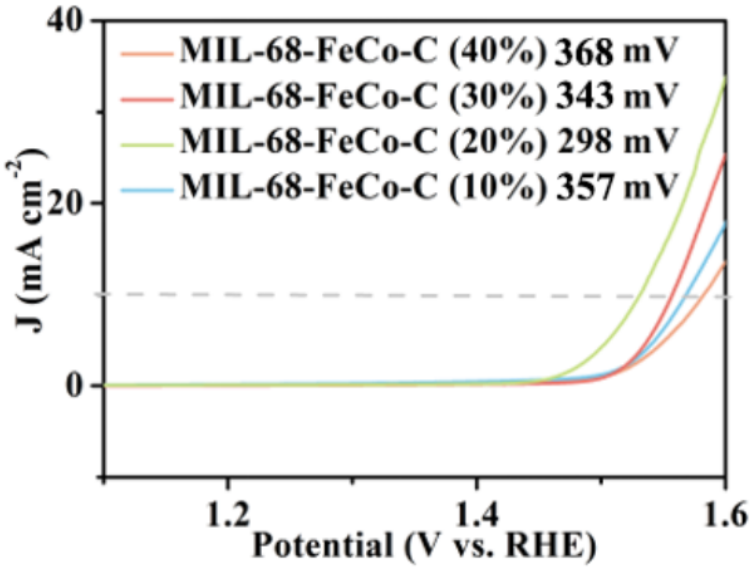

Figure S14. The LSV curves of various Fe/Co ratios in the MIL-68-FeCo-C series.

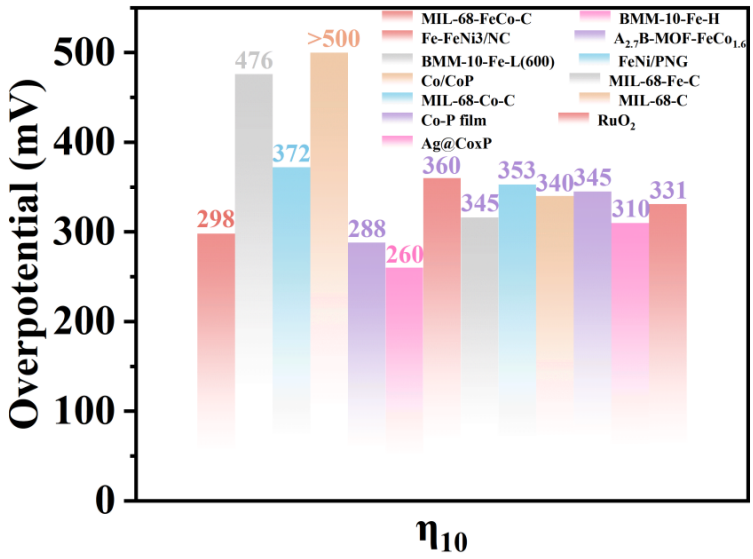

Figure S15. The η_{10} comparison of various electrocatalysts.

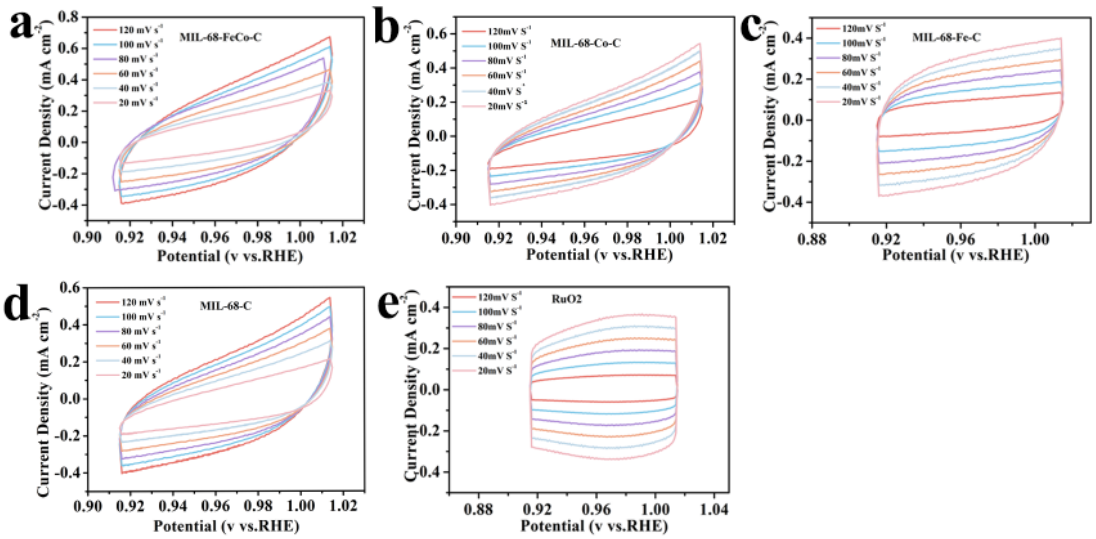

Figure S16. The CV curves from 20 to 120 mV s^{-1} of (a) MIL-68-FeCo-C; (b) MIL-68-Co-C; (c) MIL-68-Fe-C; (d) MIL-68-C and (e) RuO_2 in 1.0 M KOH.

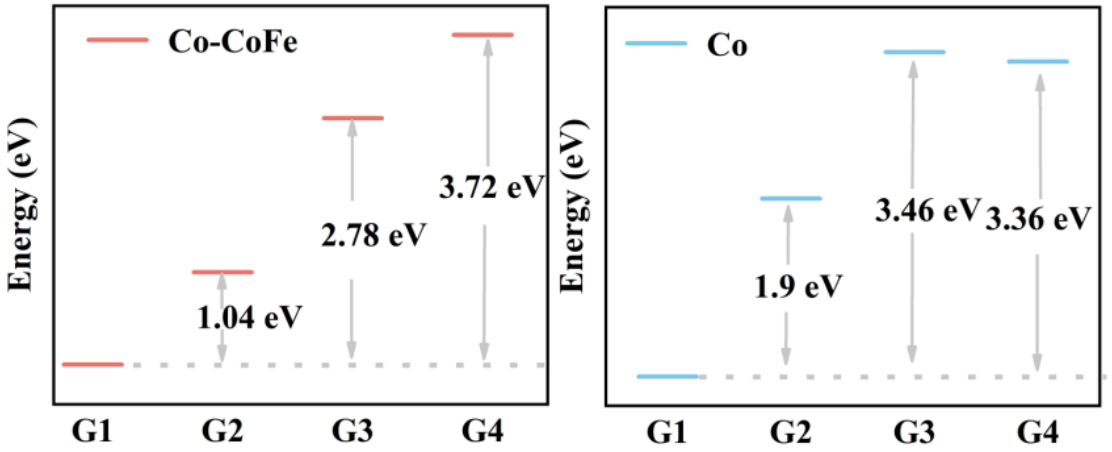

Figure S17. The calculated free energy diagrams of different surface models of Co-CoFe and Co with G1 values of 1.2 and 1.56 eV, respectively (**Ref**[1]).

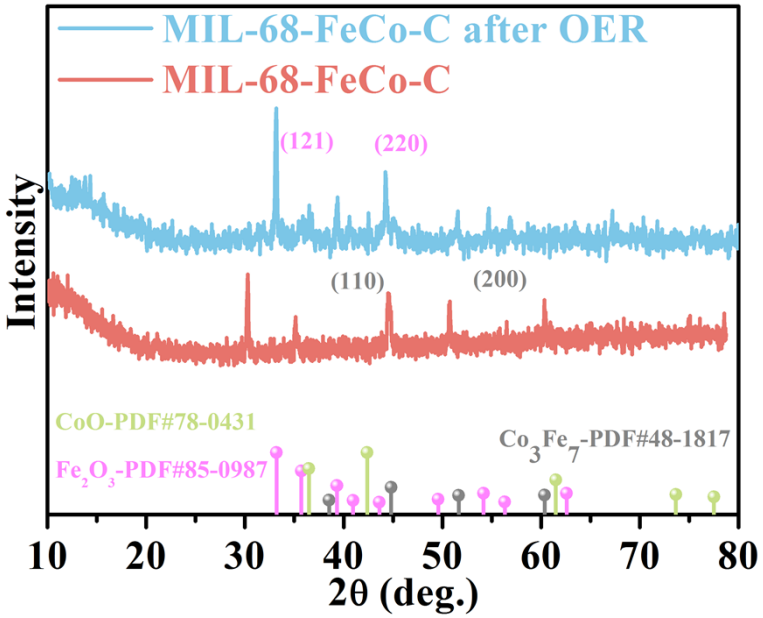

Figure S18. The PXRD patterns of MIL-68-FeCo-C before and after OER.

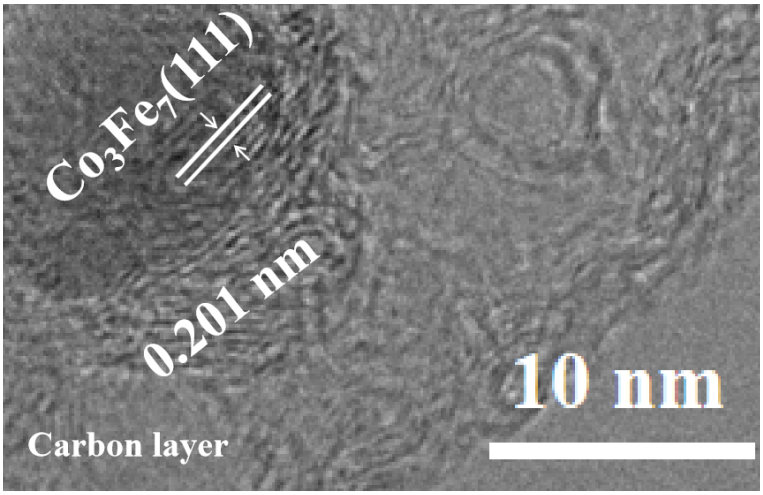

Figure S19. The TEM image of MIL-68-FeCo-C after OER.

Table S1. Crystal Data for the In-based MIL-68.

Items	MIL-68
CCDC	**1811824**
Formula	$C_{24}H_0In_3O_{15}$
Mass	733.13
crystal system	Orthorhombic
space group	*Cmcm*
a (Å)	21.892(10)
b (Å)	37.916(8)
c (Å)	7.2570(15)
α (°)	90.00
β (°)	90.00
γ (°)	90.00
V(Å^3)	6024(3)
T (K)	125(2)
Z	4
F(000)	1644
R_{int}	0.0179
R_1 (I>2σ(I))	0.0837
wR_2 (all reflections)	0.1922

Ref.[2]: For more details on the crystal structure data, please see the previously published works, *Inorganic Chemistry*, 2008, **47**, 11892-11901.

Table S2. Electrochemical Parameters of MIL-68-FeCo-C, MIL-68-Fe-C, MIL-68-Co-C, MIL-68-C, RuO_2.

Samples	η_{10} (mV)	Tafel slope (mV dec^{-1})	C_{dl} (mF cm^{-2})	R_{ct} (Ω)
MIL-68-FeCo-C	298	58.6	2.80	5.75
MIL-68-Fe-C	476	85.9	1.59	18.4
MIL-68-Co-C	372	63.3	1.28	19.0
MIL-68-C	> 500	106.7	1.16	23.2
RuO_2	331	60.7	2.26	183.8

Table S3. OER Performance Comparison between MIL-68-FeCo-C and Other Electrode Materials.

Samples	Electrolyte	η_{10} (mV)	Tafel slope (mV dec^{-1})	Reference
MIL-68-FeCo-C	**1.0 M KOH**	**298**	**58.6**	**This work**
$A_{2.7}B$-MOF-$FeCo_{1.6}$	1.0 M KOH	288	39.0	**Ref.[3]**
BMM-10-Fe-H	1.0 M KOH	260	137.4	**Ref.[4]**
FeCoSe@NCNSs	1.0 M KOH	320	95.1	**Ref.[5]**
BMM-10-Fe-L(600)	1.0 M KOH	316	119.8	**Ref.[6]**
Fe-NiO/NF	1.0 M NaOH	305	65.3	**Ref.[7]**
NP/NiO	1.0 M NaOH	332	65.6	**Ref.[8]**
CuO-NiO/NF	1.0 M NaOH	319	86.4	**Ref.[9]**
Ni-MOF@Fe-MOF	1.0 M KOH	265	82.0	**Ref.[10]**
FeNi/PNG	1.0 M KOH	353	80.0	**Ref.[11]**
Co/CoP	1.0 M KOH	340	79.5	**Ref.[12]**
Co-P film	1.0 M KOH	345	47.0	**Ref.[13]**
Ni3Fe−Co9S8/rGO	0.1 M KOH	390	109.8	**Ref.[14]**
Co_2P/CNT-900	1.0 M KOH	292	68.0	**Ref.[15]**
Ag@Co_xP	1.0 M KOH	310	76.4	**Ref.[16]**
Fe-FeNi3/NC	0.1 M KOH	360	82.0	**Ref.[17]**

The loading mass of the catalyst in this work is 0.85 mg cm^{-2}.

References

1. J. Chen, H. Li, S. Chen, J. Fei, C. Liu, Z. Yu, K. Shin, Z. Liu, L. Song, G. Henkelman, L. Wei and Y. Chen, *Advanced Energy Materials*, 2021, **11**, 2003412, 1614-6832.
2. C. Volkringer, M. Meddouri, T. Loiseau, N. Guillou, J. Marrot, G. Férey, M. Haouas, F. Taulelle, N. Audebrand and M. Latroche, *Inorganic Chemistry*, 2008, **47**, 11892-11901, 0020-1669.
3. Z. Xue, Y. Li, Y. Zhang, W. Geng, B. Jia, J. Tang, S. Bao, H.-P. Wang, Y. Fan, Z.-w. Wei, Z. Zhang, Z. Ke, G. Li and C.-Y. Su, *Advanced Energy Materials*, 2018, **8**, 1801564, 1614-6832.
4. J. Ding, Q. Sun, L. Zhong, X. Wang, L. Chai, Q. Li, T.-T. Li, Y. Hu, J. Qian and S. Huang, *Electrochimica Acta*, 2020, **354**, 136716, 0013-4686.
5. Y. Pan, M. Wang, M. Li, G. Sun, Y. Chen, Y. Liu, W. Zhu and B. Wang, *Journal of Energy Chemistry*, 2022, **68**, 699-708, 20954956.
6. L. Zhong, X. Wang, Y. Guo, J. Ding, Q. Huang, T.-T. Li, Y. Hu, J. Qian and S. Huang, *ACS Applied Materials & Interfaces*, 2021, **13**, 55454-55462, 1944-8244.
7. Z. Qiu, Y. Ma and T. Edvinsson, *Nano Energy*, 2019, **66**, 22112855.
8. D. Xiong, C. Lu, C. Chen, J. Wang, Y. Kong, T. Liu, S. Ying and F.-Y. Yi, *Journal of Power Sources*, 2022, **520**, 03787753.
9. Z. Wang, J. Ang, B. Zhang, Y. Zhang, X. Y. D. Ma, T. Yan, J. Liu, B. Che, Y. Huang and X. Lu, *Applied Catalysis B: Environmental*, 2019, **254**, 26-36, 09263373.
10. K. Rui, G. Zhao, Y. Chen, Y. Lin, Q. Zhou, J. Chen, J. Zhu, W. Sun, W. Huang and S. X. Dou, *Advanced Functional Materials*, 2018, **28**, 1616-301X 1616-3028.
11. H. Wang, X. Feng, M. Zhou, X. Bo and L. Guo, *ACS Applied Nano Materials*, 2020, **3**, 6336-6343
12. Z.-H. Xue, H. Su, Q.-Y. Yu, B. Zhang, H.-H. Wang, X.-H. Li and J.-S. Chen, *Advanced Energy Materials*, 2017, **7**, 16146832.
13. N. Jiang, B. You, M. Sheng and Y. Sun, *Angewandte Chemie International Edition*, 2015, **54**, 6251-6254, 14337851.
14. X. Hu, T. Huang, Y. Tang, G. Fu and J.-M. Lee, *ACS Applied Materials & Interfaces*, 2019, **11**, 4028-4036, 1944-8244.
15. D. Das and K. K. Nanda, *Nano Energy*, 2016, **30**, 303-311, 22112855.
16. Y. Hou, Y. Liu, R. Gao, Q. Li, H. Guo, A. Goswami, R. Zboril, M. B. Gawande and X. Zou, *ACS Catalysis*, 2017, **7**, 7038-7042, 2155-5435 2155-5435.
17. K. Chen, S. Kim, R. Rajendiran, K. Prabakar, G. Li, Z. Shi, C. Jeong, J. Kang and O. L. Li, *Journal of Colloid and Interface Science*, 2021, **582**, 977-990, 0021-9797.